Chapter 2

PHASAR demultiplexers: a review

Wavelength multiplexers, demultiplexers and routers based on optical phased arrays play a key role in multiwavelength telecommunication links and networks. In this chapter a detailed description of phased-array operation and design is presented and an overview is given of the most important applications. Part of this work has also been published in the Journal of Selected Topics in Quantum Electronics [118].

2.1 Basic operation

Figure 2.1a shows the schematic layout of a PHASAR-demultiplexer. The operation is understood as follows. When the beam propagating through the transmitter waveguide enters the Free Propagation Region (FPR), it is no longer laterally confined and becomes divergent. On arriving at the input aperture, the beam is coupled into the waveguide array and propagates through the individual array waveguides towards the output aperture. The length of the array waveguides is chosen in such a way that the optical path length difference between adjacent waveguides equals an integer multiple of the central wavelength of the demultiplexer. For this wavelength the fields in the individual waveguides will arrive at the output aperture with equal phase (apart from an integer multiple of 2π), and the field distribution at the input aperture will be reproduced at the output aperture. The divergent beam at the input aperture is thus transformed into a convergent one with equal amplitude and phase distribution, and an image of the input field at the object plane will be formed at the centre of the image plane. The dispersion of the PHASAR is due to the linearly increasing length of the array waveguides, which will cause the phase change induced by a change in the wavelength to vary linearly along the output aperture. As a consequence, the outgoing beam will be tilted and the focal point will shift along the image plane. By placing receiver waveguides at proper positions along the image plane, spatial separation of the different wavelength channels is obtained.
In the following subsections the most important properties of a PHASAR will be analysed.

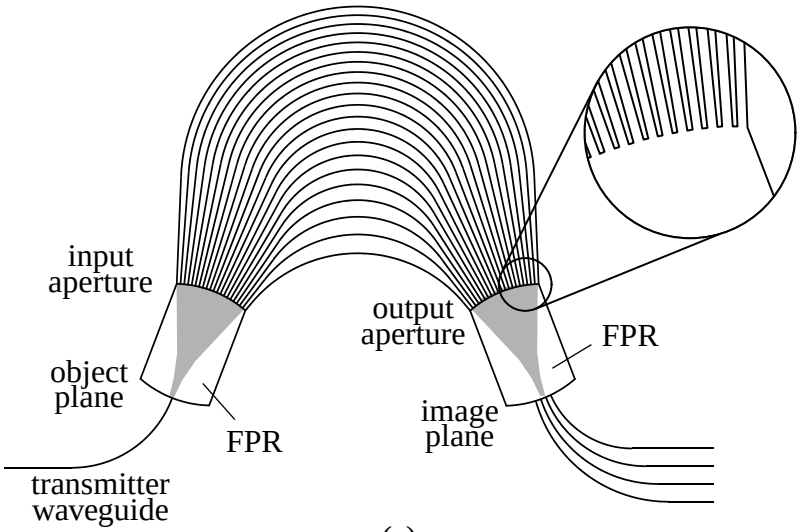

(a)

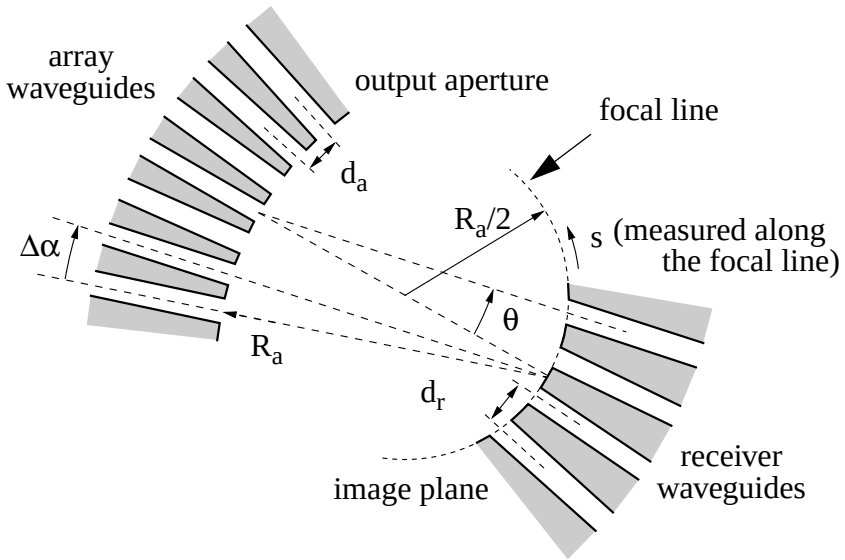

(b)

Figure 2.1 a) Layout of the PHASAR demultiplexer
b) Geometry of the receiver side.

2.1.1 Focusing

Focusing is obtained by choosing the length difference ΔL between adjacent array waveguides equal to an integer number of wavelengths, measured inside the array waveguides:

$$\Delta L = m \cdot \frac{\lambda_c}{N_{eff}} = \frac{mc}{N_{eff} f_c} \tag{2.1}$$

whereby m is the order of the phased array, λ_c (f_c) is the central wavelength (frequency) in vacuo and N_{eff} is the effective index of the waveguide mode. With this choice the array acts as

a lens with image and object planes at a distance R_a of the array apertures.
The input and output apertures of the phased array are typical examples of Rowland-type mountings [81]. The focal line of such a mounting, which defines the image plane, follows a circle with radius $R_a/2$ as shown in figure 1b. Transmitter and receiver waveguides should be positioned on this line.

α/α_i	starting angle/starting angle of array waveguide *i*
α_r	reference angle
β/β_{FPR}	propagation constant in waveguide/FPR
c	speed of light
D	dispersion
d_a	pitch of the array waveguides in the array aperture
d_r	pitch of the receiver waveguides in the image plane
$\Delta\alpha$	divergence angle of the array waveguides in the array aperture
Δf_{ch}	channel spacing
Δf_{FSR}	free spectral range
Δf_{pol}	TE-TM shift
Δf_L	*L*-dB bandwidth
$\Delta\Phi$	phase shift between adjacent array waveguides
ΔL	path length difference between adjacent array waveguides
H_i	height of array waveguide *i*
k_0	wave number in vacuo
L	distance between the focal points
L_o	central channel insertion loss
L_p	propagation loss in the array
L_u	non-uniformity
$l(\alpha)$	path length of array waveguide with respect to α
l_i	path length of array waveguide *i*
λ_c/f_c	central (design) wavelength/frequency
m/m'	order of the array/beam
N/N_a	number of channels/array waveguides
N_{eff}/N_{FPR}	effective index in waveguide/FPR
N_g	group index
N_{TE}/N_{TM}	effective index for TE/TM polarisation
N_1/N_2	transverse effective index in the ridge/in the region next to the ridge
R_a	length of FPR
R_i	radius of curvature of array waveguide *i*
R_r	radius of curvature of reference array waveguide
S_i	straigth section length (including R_a) of array waveguide *i*
S_r	straigth section length (including R_r) of reference array waveguide
s	position along image plane
θ	dispersion angle
θ_a	array aperture half angle
θ_o	angular width of the far field
V	lateral *V*-parameter (normalised film parameter)
w/w_e	waveguide width/effective width

Table 2.1 List of symbols used in this chapter.

2.1.2 Dispersion and Free Spectral Range

In figure 2.1b it can be seen that the dispersion angle θ resulting from a phase difference ΔΦ between adjacent waveguides follows as:

$$\theta = \arcsin\left(\frac{(\Delta\Phi - m2\pi)/\beta_{FPR}}{d_a}\right) \approx \frac{\Delta\Phi - m2\pi}{\beta_{FPR} d_a} \tag{2.2}$$

whereby $\Delta\Phi = \beta\Delta L$, β and β_{FPR} are the propagation constants in the array waveguide and the Free Propagation Region (FPR) respectively, and d_a is the lateral spacing (on centre lines) of the waveguides in the array aperture.
The dispersion D of the array is described as the lateral displacement ds of the focal spot along the image plane per unit frequency change. From figure 2.1b it follows (after some manipulation, see Appendix B) that:

$$D = \frac{\mathrm{d}s}{\mathrm{d}f} = R_a \cdot \frac{\mathrm{d}\theta}{\mathrm{d}f} = \frac{1}{f_c} \cdot \frac{N_g}{N_{FPR}} \cdot \frac{\Delta L}{\Delta\alpha} \tag{2.3}$$

whereby $f_c = c/\lambda_c$ is the central frequency, N_{FPR} is the (slab) mode index in the Free Propagation Region, ΔL is the length increment of the array waveguides as described before, $\Delta\alpha = d_a/R_a$ is the divergence angle between the array waveguides in the fan-in and fan-out sections and N_g is the group index of the waveguide mode:

$$N_g = N_{eff} + f\frac{\mathrm{d}N_{eff}}{\mathrm{d}f} \tag{2.4}$$

It can be seen that R_a does not occur in the right hand expression in equation 2.3 so that filling-in of the space between the array waveguides near the apertures due to a finite lithographical resolution does not affect the dispersive properties of the demultiplexer.
From equation 2.2 it can be seen that the response of the phased array is periodical. After each change of 2π in ΔΦ, the field will be imaged at the same position. The period in the frequency domain as shown in figure 2.2b is called the Free Spectral Range (FSR). It is found as the frequency shift for which the phase shift ΔΦ equals 2π:

$$\frac{2\pi\Delta f_{FSR}}{c} N_g \Delta L = 2\pi \tag{2.5}$$

from which we derive:

$$\Delta f_{FSR} = \frac{c}{N_g \Delta L} = \frac{f_c}{m'} \tag{2.6}$$

with $m' = (N_g/N_{eff}) \cdot m$.
The rightmost identity, which is well known from grating theory, follows by substituting $N_g\Delta L = m'c/f_c$ (see equation 2.1). It is noted that for phased arrays, different from gratings, the Free Spectral Range is not related to the order m of the array, but to a modified order number m', which can be interpreted as the order of the beam.
As the exact relation between θ and ΔΦ is non-linear (see equation 2.2), equation 2.6 is only approximate and the FSR will be slightly dependent on the input and output ports. An accurate analysis is given by Takahashi et al. [155].

2.1.3 Insertion loss and non-uniformity

Figure 2.2a shows the field in the image plane for four different wavelengths. It is the sum field of the far fields of all individual array waveguides. As the far-field intensity of the individual waveguides reduces away from the centre of the image plane, as indicated in the figure, the focal sum field will do the same. If the wavelength is changed, it will move through the image plane and follow the envelope described by the far-field of the individual array waveguides. If we approximate the modal field of the array waveguides as a Gaussian beam and neglect the effects of coupling on the beam shape, we can derive some simple analytical equations for estimating insertion loss, channel non-uniformity and bandwidth.
Using the Gaussian-beam approximation, the intensity of the far-field is found in:

$$I(\theta) = I_o e^{-2\theta^2/\theta_o^2} \tag{2.7}$$

whereby θ_o is the width of the equivalent Gaussian far field

$$\theta_o = \frac{\lambda}{N_{FPR}} \cdot \frac{1}{w_e\sqrt{2\pi}} \tag{2.8}$$

with w_e being the effective width of the modal field in the transmitter waveguide (as described in Appendix C). The non-uniformity L_u is defined as the intensity ratio (in dB) between the outer and the central channel. Using equation 2.7, the insertion loss of the receiver relative to the central channel is easily found by substituting the angle θ_{max} ($\theta_{max} \approx s_{max}/R_a$) corresponding to the outer receiver waveguide:

$$L_u = -10 \cdot \log\left(e^{-2\theta_{max}^2/\theta_o^2}\right) \approx 8.7 \cdot \theta_{max}^2/\theta_o^2 \tag{2.9}$$

If the FSR is chosen as being equal to N times the channel spacing Δf, as in wavelength routers (see section 2.3.1), the excess loss L_u of the outer channels will be close to 3 dB for reasons of power conservation - as for large numbers of channels, receiver waveguide 1 and the virtual receiver N+1 will experience approximately the same loss with each of them having at least 3 dB excess loss relative to the central channel. For small values of N the situation may be slightly better. Thus minimising L_u will increase the FSR.
The insertion loss L_o of the central channel is mainly determined by diffraction of light into undesired orders. The adjacent orders of the main focal spot will carry a fraction $\exp(-2\Delta\theta_{FSR}^2/\theta_o^2)$, with:

$$\Delta\theta_{FSR} = \frac{\Delta s_{FSR}}{R_a} = \frac{D}{R_a}\Delta f_{FSR} \tag{2.10}$$

whereby D is the dispersion (equation 2.3). If we neglect the power coupled into other orders the total loss L_o can be estimated from:

$$L_o \approx -10 \cdot \log\left(1 - 4 \cdot e^{-2\Delta\theta_{FSR}^2/\theta_o^2}\right) + L_p \approx 17 \cdot e^{-4\pi w_e^2/d_a^2} + L_p \tag{2.11}$$

whereby it has been assumed that $\exp(-2\Delta\theta_{FSR}^2/\theta_o^2) \ll 1$. The factor 4 is due to the fact that

power is lost in two orders and that equal losses occur (because of reciprocity) at both the input and the output side of the array. The term L_p denotes the total propagation loss in the array and both FPRs due to absorption and scattering. From this equation it can be seen that for low-loss devices the waveguide spacing d_a in the array apertures should be minimal. For semiconductor-based devices, the best total loss reported is in the order of 2 dB [141]. It should be noted that equation 2.11 is a worst-case guess - coupling between the array waveguides will reduce the loss as discussed in section 2.2.6.

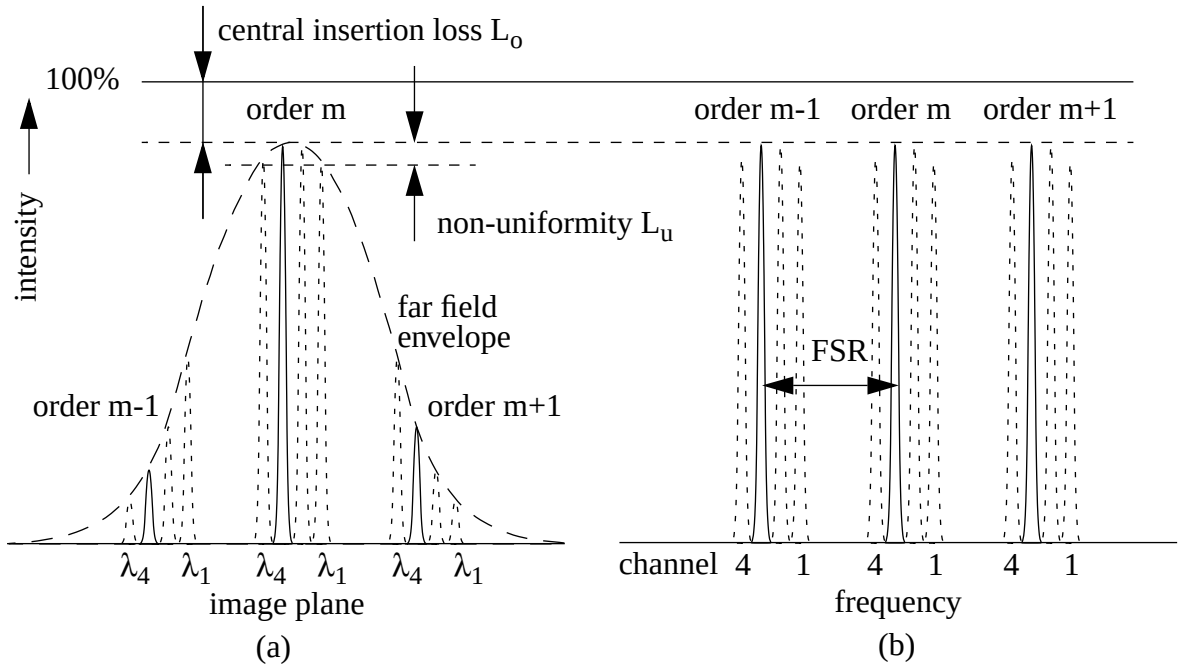

Figure 2.2 Central insertion loss, non-uniformity and free spectral range (FSR). The 100% line denotes the peak intensity of the input field.

2.1.4 Bandwidth

If the wavelength is changed, the focal field of the PHASAR moves along the receiver waveguides. The frequency response of the different channels follows from the overlap of this field with the modal fields of the receiver waveguides. If we assume that the focal field is a good replica of the modal field at the input, and that the input and output waveguides are identical, the (logarithmic) transmission $T(\Delta f)$ around the channel maximum $T(f_c)$ follows as the overlap of the modal field with itself, displaced over a distance $\Delta s(\Delta f) = D\Delta f$:

$$T(\Delta f) = T(f_c) + 20\log\int_{-\infty}^{+\infty} U(s)U(s-D\Delta f)\mathrm{d}s \qquad (2.12)$$

whereby $U(s)$ is the normalised modal field, D is the dispersion as defined in equation 2.3 and $T(f_c)$ is the transmission in dB at the channel maximum. For small values of Δs (smaller than the effective mode width w_e) the overlap integral can be evaluated analytically by

approximating the modal fields as Gaussian fields:

$$T(\Delta f) - T(f_c) = 20 \cdot \log\left(\exp\left(-\frac{D\Delta f^2}{w_o^2}\right)\right) \approx -6.8 \cdot \left(\frac{D\Delta f}{w_e}\right)^2 \qquad (2.13)$$

The L-dB bandwidth Δf_L is twice the value Δf for which $T(\Delta f) - T(f_c) = L$ dB:

$$\Delta f_L = 0.77\frac{w_e}{D}\sqrt{L} = 0.77\frac{w_e}{d_r}\Delta f_{ch}\sqrt{L} \qquad (2.14)$$

The latter identity follows by substitution of $D = d_r/\Delta f_{ch}$. If we substitute $w_e/d_r \approx 0.4$ as a representative value (cross talk due to receiver waveguide spacing <-40 dB, see section 2.1.5), the 1-dB bandwidth is found to be $0.31 \cdot \Delta f_{ch}$. For a channel spacing of 100 GHz we find a 1-dB bandwidth of 31 GHz. A special case of bandwidth usage was applied by Okamoto et al. [92], who produced a variable bandwidth filter. Different waveguide widths are used for the transmitter waveguides and the same widths are anti-symmetrically used for the receiver waveguides. In this way, the centre frequency of the filter is identical for all channels, only the bandwidth is different.

2.1.5 Channel cross talk

Cross talk may be caused by many mechanisms. We will discuss six of them. The first four can be kept low by proper design. The other two follow from imperfections during the production process and are more difficult to reduce.
It is usual in the literature on WDM devices to characterise the cross talk performance by specifying the single channel cross talk figure, i.e. the maximum cross talk value which is measured with one active input channel. Under operating conditions the cross talk will be higher than this value, as all active input channels will contribute to it. An analysis of the cross talk penalty under simultaneous multichannel operation is given by Takahashi et al. [155].

Receiver waveguide cross talk
The most obvious source of cross talk is the coupling between the receiver waveguides through the exponential tails of the field distributions. This type of cross talk follows directly from equation 2.12. Because we are now looking at the coupling through the exponential tails of the modal field, the Gaussian approximation is not valid and the integral should be evaluated using the expressions for the (normalised) mode profile. Figure 2.3a shows the cross talk due to overlapping fields, calculated for different values of the lateral V-parameter, which is defined as:

$$V = k_0 w \sqrt{N_1^2 - N_2^2} \qquad (2.15)$$

whereby k_0 is the wave number in vacuo, w the waveguide width, and N_1,N_2 the transverse effective indices in ridge and in the region next to the ridge respectively.
The curves are almost polarisation independent. Note that with polarisation dependent waveguides the lateral V-parameter will be polarisation dependent.

Truncation

Another source of cross talk results from truncation of the field due to the finite width of the array aperture. This causes power to be lost at the input aperture, whilst at the output aperture the side lobe level of the focal field will increase. For a proper PHASAR design, the array aperture angle should be chosen in such a way that the corresponding cross talk is sufficiently low. Figure 2.3b shows the transmitted power (solid line) and the cross talk versus the array aperture half angle θ_a, defined as:

$$\theta_a = \frac{(N_a - 1)d_a}{2R_a} \tag{2.16}$$

normalised to the Gaussian width θ_o as defined in equation 2.8, for different values of the relative receiver waveguide spacing d_r/w. As the estimate of figure 2.3a is rather pessimistic, it is best to use the envelope depicted by the boldly dashed line. The values shown are calculated for input and output waveguides with $V = 3$. The dependence on the V-parameter is small. The envelope of the cross talk curves (boldly dashed line) can be used for estimating the maximum cross talk level. It is seen that for $\theta_a > 2\theta_o$ the truncation cross talk is less than -35 dB.

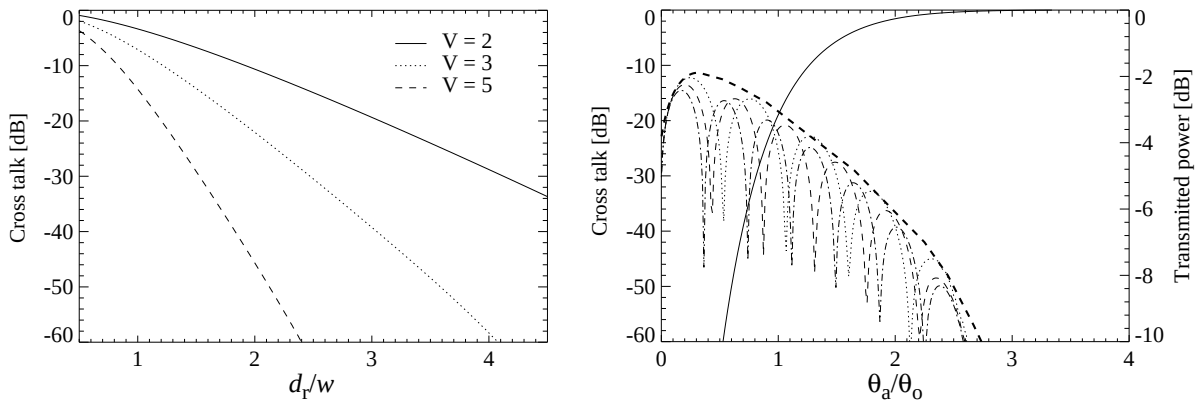

(a) (b)

Figure 2.3 a) Cross talk resulting from the coupling between two adjacent receiver waveguides for different values of the lateral V-parameter of the receiver waveguides.

b) Transmitted power (solid line) and cross talk as a function of the relative array aperture θ_a/θ_o, for different values of the relative receiver waveguide spacing d_r/w (d_r/w = 2.5, 3.0, 3.5). The values shown are calculated for input and output waveguides with $V = 3$. The boldly dashed line indicates the envelope of the cross talk curves (maximum cross talk level).

Mode conversion

If the array waveguides are not strictly single mode, a first order mode excited at the junctions between straight and curved waveguides can propagate coherently through the array and cause "ghost" images. Because of the difference in the propagation constant between the fundamental and the first order mode, these images will occur at different locations and the "ghost image" may couple to an undesired receiver waveguide thereby degrading the cross talk performance. Mode conversion can be kept small by optimising the offset at the junctions for minimal first-order mode excitation.

Coupling within the array
Cross talk can also be incurred by phase distortion due to coupling in the input and output sections in the arrays. It might be expected that this type of coupling will not greatly affect the focusing and dispersive properties of the array on similar grounds as to those mentioned in equations 2.3 and 2.4. The filling in of the gaps near the array apertures can be considered as introducing an extremely strong coupling into the input and output region, which obviously does not degrade the PHASAR performance [117]. Day et al. [38], however, observe a degradation of the cross talk performance using BPM-simulation.

Phase transfer errors
A fifth source of cross talk results from phase transfer errors in the phased array due to imperfections during the production process. The optical path length of the array guides is in the order of several thousands of wavelengths. Deviations in the propagation constant may lead to considerable errors in the phase transfer, and, consequently, to an increase of the cross talk level. Takada et al. [150] and Yamada et al. [170,171] have shown that improved cross talk is feasible by correcting the phase errors (e.g. by using thin-film heaters on top of the array waveguides). Phase errors may be caused by small deviations in the effective index due to local variations in composition, film thickness or waveguide width, or by inhomogeneous filling in of the gap near the apertures of the phased array. Also more systematic errors (e.g. due to discretisation in the mask pattern generation) may contribute to the cross talk [38].

Background radiation
As a last possible source of cross talk we mention background radiation due to light scattered out of the waveguides at junctions or rough waveguide edges. This is especially important in waveguide structures where the light is also guided besides the waveguides e.g. in shallow etched ridge guides or in waveguide structures on a heavily doped substrate where the undoped buffer layer may also act as a waveguide.

Cross talk in practical devices is not limited by design but by imperfections during the production process. Typical cross talk values reported for PHASAR-demultiplexers are in the order of -25 dB for InP-based devices to even less than -30 dB for silica-based devices. Recent experiments in our laboratory, however, show cross talk levels less than -30 dB for good semiconductor devices as well, which is outlined in Appendix D. Improvement on these figures is mainly a matter of improving manufacturing technology.

2.1.6 Polarisation dependence

Phased arrays are polarisation independent if the array waveguides are polarisation independent, i.e. the propagation constants for the fundamental TE- and TM-mode are equal. Waveguide birefringence, i.e. a difference in propagation constants, will result in a shift Δf_{pol} of the spectral responses in respect of each other, which is called the polarisation dispersion. It can be calculated when we consider the effective wavelengths in the waveguide. Light with different wavelengths *in vacuo* will be coupled into the same receiver waveguide, when the effective wavelengths λ_{TE} and λ_{TM} of the fundamental modes in the waveguide are equal:

$$\lambda_{\mathrm{TM}}(f) = \frac{c}{f \cdot N_{\mathrm{TM}}(f)} = \lambda_{\mathrm{TE}}(f - \Delta f_{\mathrm{pol}}) = \frac{c}{(f - \Delta f_{\mathrm{pol}}) \cdot N_{\mathrm{TE}}(f - \Delta f_{\mathrm{pol}})} \quad (2.17)$$

whereby N_{TE} and N_{TM} are the effective indices for both polarisations.

By solving Δf_{pol} from equation 2.17 we find:

$$\Delta f_{pol} \approx f \cdot \frac{(N_{TE} - N_{TM})}{N_{g,TE}} \tag{2.18}$$

whereby $N_{g,TE}$ is the group index. For InGaAsP/InP DH waveguide structures, Δf_{pol} is typically in the order of 4-5 nm. For silica-based and, more generally, for low-contrast waveguides, it will be much smaller. Also, in waveguides structures which are designed for polarisation independence, polarisation dependence may occur due to strain induced during the manufacturing process. A number of methods to reduce polarisation dependence will be mentioned briefly in section 2.2.4, and will be discussed more comprehensively in Chapter 4.

2.2 Phased-array design

2.2.1 Specification

A PHASAR is specified by the following characteristics:
- Number of channels N.
- Central frequency f_c and channel spacing Δf_{ch}.
- L-dB Channel bandwidth Δf_L.
- Free Spectral Range Δf_{FSR}.
- Maximal insertion loss L_o of the central channel.
- Maximal non-uniformity L_u.
- Maximal cross talk level.
- Maximal polarisation dependence.

It is noted that the non-uniformity and the Free Spectral Range can not be chosen independently from each other (see section 2.3.1)

2.2.2 Demultiplexer design procedure

PHASARs have many degrees of design freedom and many design approaches are possible. The approach followed at TU Delft for designing multiplexers and demultiplexers is explained below. It starts with a given waveguide structure (i.e. waveguide width w and lateral V-parameter fixed). The design parameters of the PHASAR are derived subsequently from the design specifications. The design procedure of a wavelength router is slightly different (see section 2.3.1). For the reader's convenience figure 2.1b is shown here again.

- **Receiver waveguide spacing d_r.** We start with the cross talk specification, which puts a lower limit on the receiver waveguide spacing d_r. As with today's technology cross talk levels lower than -30 to -35 dB are difficult to realise, it does not make sense to design the array for much lower cross talk. To be on the safe side, we take a margin of 5-10 dB and read from figure 2.3a the ratio d_r/w required for -40 dB cross talk level. It is noted that the cross talk for TE- and TM-polarisation may be different as the lateral index contrast and, consequently, the lateral V-parameter can differ substantially for the two polarisations.
- **FPR length R_a.** From the maximum acceptable excess loss for the outer channel (the non-uniformity L_u), we determine the maximum acceptable dispersion angle θ_{max} using equations 2.8 and 2.9. The minimal length $R_{a,min}$ of the Free Propagation Region then follows as $R_{a,min} = s_{max} / \theta_{max}$ whereby s_{max} is the s-coordinate of the outer receiver waveguide (see figure 2.1b).

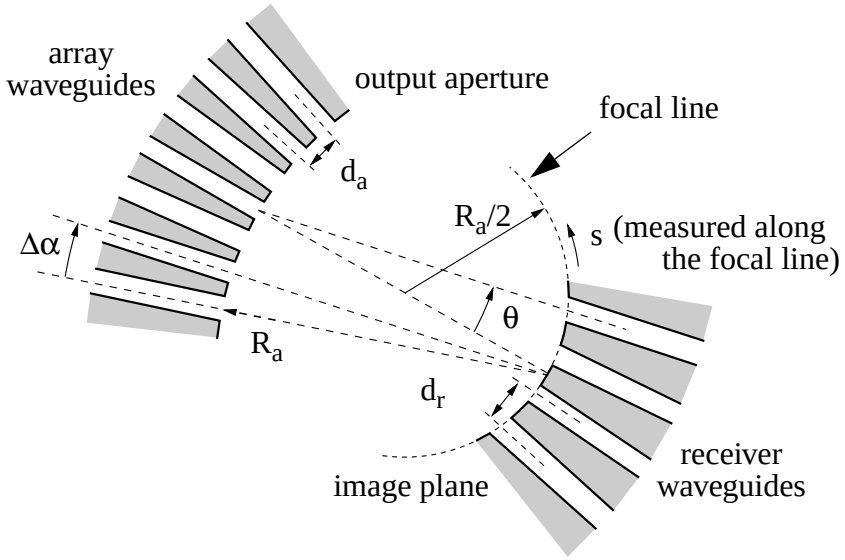

Figure 2.4 Geometry of the receiver side of a PHASAR demultiplexer.

- **Length increment ΔL**. First we compute the required dispersion of the array from $D = \mathrm{d}s/\mathrm{d}f = d_r/\Delta f_{ch}$ (see equation 2.3). The waveguide spacing d_a in the array aperture should be chosen as small as possible (a large spacing will lead to high coupling losses from the FPR to the array and vice versa). With d_a and R_a fixed, the divergence angle $\Delta\alpha$ between the array waveguides is fixed as $\Delta\alpha = d_a/R_a$ (see figure 2.1b) and the length increment ΔL of the array follows from equation 2.3.
- **Aperture width θ_a**. The angular half width θ_a of the array aperture should be determined using a graph like figure 2.3b (adapted for the specific waveguide structure used).
- **Number of array waveguides N_a**. The choice of θ_a fixes the number of array waveguides: $N_a = 2\theta_a R_a/d_a + 1$ (see equation 2.16).

This completes the determination of the most important geometrical parameters of the PHASAR.

2.2.3 Array geometry

For the array waveguides a number of different shapes can be applied to realise the length increment ΔL. Takahashi et al. [152] used the geometry as depicted in figure 2.5a, which is very simple from a design point of view, with a constant R for all array arms. Smit [117] and Dragone [44] applied the geometry of figure 2.5b, which contains a minimum number of waveguide junctions. This is especially important in semiconductor waveguides where junction losses and mode conversion at junctions can degrade the PHASAR performance.

The freedom in the choice of array shape is bounded by the requirement that the array waveguides should not come too close to each other. For extremely low dispersion values (e.g. for duplexing 1.3 and 1.55 μm), the path length difference ΔL between adjacent waveguides becomes very small and the shapes depicted in figure 2.5 are no longer suitable. Adar et al. [1] applied S-bend-like arrays in which the dispersion of one curved section is reduced by a second section with opposite curvature and, consequently, opposite ΔL. Mestric et al. [83,84] recently also reported a S-bend shaped phased-array 1.31-1.55 μm duplexer with very low cross talk (<-30 dB) and extremely small dimensions (0.5×0.2 mm^2).

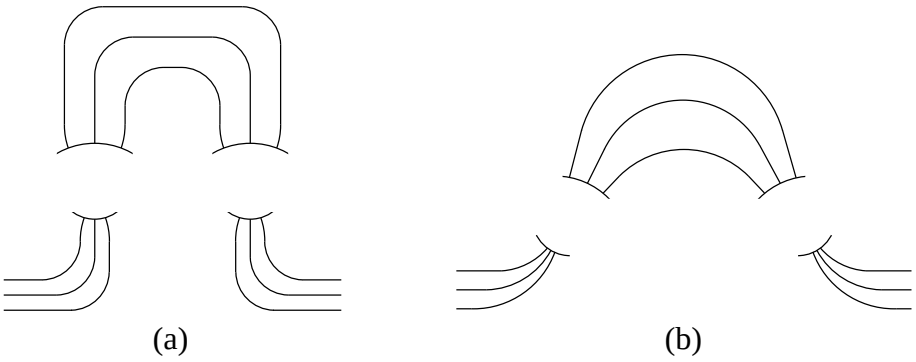

Figure 2.5 Phased-array waveguide geometries.

The geometry as shown in figure 2.5b is also used for the design of the phased-array demultiplexers discussed in this thesis and will be described below. According to this geometry, an array guide consists of two straight waveguides connected to each other by a curved waveguide, together forming a non-concentric set.

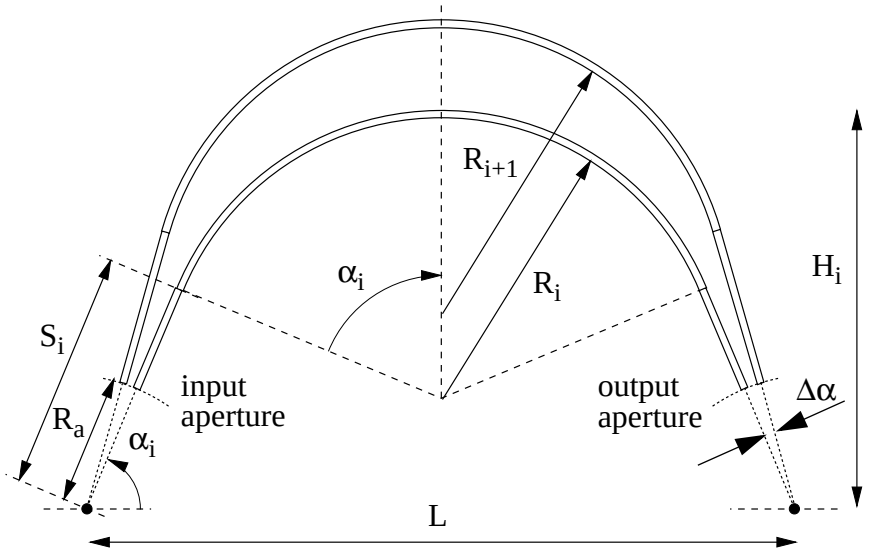

Figure 2.6 Geometry of the *i*-th guide of the phased-array.

Each array guide is completely defined by the starting angle α_i, the radius of curvature R_i and the straight section length S_i, which includes the focal length R_a for ease of calculation, according to:

$$R_i = \frac{L/2 - S_i \cos\alpha_i}{\sin\alpha_i} \tag{2.19}$$

$$S_i = \frac{1}{2}\left(l_i - \frac{L\alpha_i}{\sin\alpha_i}\right) \Big/ \left(1 - \frac{\alpha_i \cos\alpha_i}{\sin\alpha_i}\right) \tag{2.20}$$

and:

$$\alpha_i = \alpha_1 + (i-1)\Delta\alpha \tag{2.21}$$

whereby l_i is the path length of the i-th array guide measured from transmitter to receiver:

$$l_i = l_1 + (i-1)\Delta L \tag{2.22}$$

In the above equations $\Delta\alpha$ is the divergence angle of the array waveguides in the array aperture and ΔL is the path length difference between adjacent array waveguides.

2.2.4 Design for polarisation independence

Several methods can be used for eliminating the polarisation dependence of the response due to waveguide birefringence. Five different methods will be briefly discussed here and more comprehensively in Chapter 4.

Nonbirefringent waveguides

The most obvious way to make a PHASAR polarisation independent is by eliminating the birefringence of the waveguide. This can be done by making the waveguide cross section square if the index contrast is the same in both the vertical and lateral direction as, for example, in buried waveguide structures. Bellcore [11,123] recently reported a polarisation independent device based on a buried InGaAsP/InP waveguide structure with a low-contrast waveguide core (small InGaAs-fraction). Philips and TU Delft, Bellcore, and Alcatel [9,19,20,21,122, 164] reported several devices based on a raised strip guide using similar material for the waveguide core. An advantage of the raised strip guide is that, due to the high lateral index contrast, it allows for very short bending radii and, consequently, for compact design. This method will be discussed more comprehensively in Chapter 4.

Attempts have been made to compensate the birefringence of conventional “flat” waveguide structures by applying strained MQW-waveguides. Bi-axial compressive strain, obtained by decreasing the Ga-fraction, increases the birefringence, whereas bi-axial tensile strain reduces it. First results of this method show that polarisation dispersion changes in the order of 7-12 nm are possible [166]. A complication of this approach is that the intrinsic birefringence of MQW-structures is considerably higher than that of quaternary bulk material and requires very high strains for it to be compensated. This makes the approach sensitive to well-width and composition control.

The birefringence problem occurs also in silica-based waveguides, where it is due to strain induced by the different thermal expansion coefficients of silica and silicon. It can be reduced by using silica substrates instead of silicon substrates [142].

Order matching

The first attempt to make PHASARs polarisation independent was based on matching the FSR to the polarisation dispersion as shown in figure 2.7 [127,133,162,163,177]. If the FSR is chosen to be equal to the polarisation dispersion the m-th order beam for TE will overlap with the TM-polarised beam of order m-1, which makes the response virtually polarisation independent. From equation 2.6 it can be seen that this is obtained by choosing:

$$\Delta L = \frac{c}{N_g \Delta f_{pol}} \tag{2.23}$$

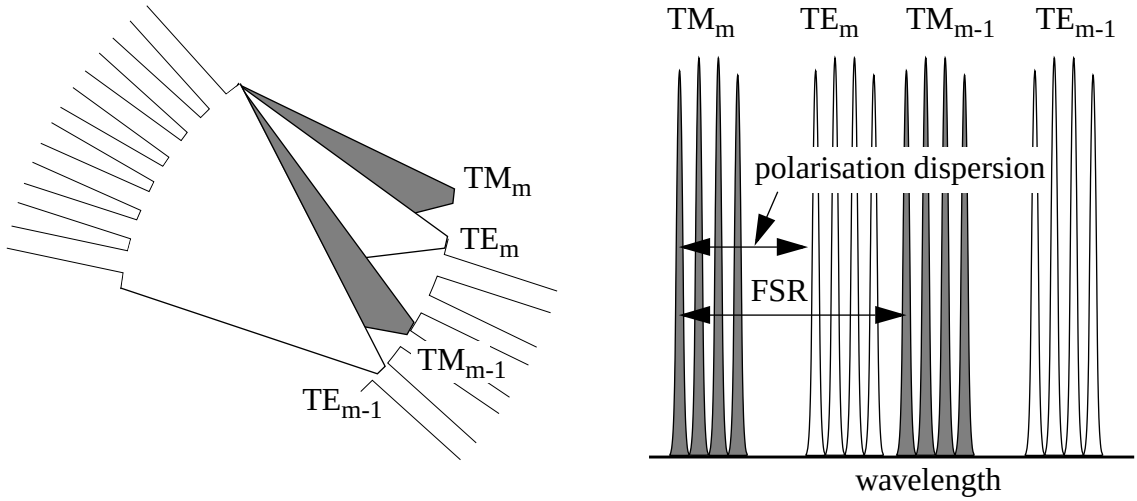

Figure 2.7 Schematic diagram of the different diffraction orders at the receiver side for both states of polarisation: polarisation dispersion. The diagram applies to the demultiplexer's state *without* order matching, because the orders TE_m and TM_{m-1} do not overlap.

For this design, the procedure described in section 2.2.2 should be slightly changed. By fixing the incremental length according to equation 2.23, the divergence angle $\Delta\alpha$ is fixed through equation 2.3 and R_a through $R_a = d_a/\Delta\alpha$ (see figure 2.1b). R_a being fixed in this way, the non-uniformity L_u can no longer be freely chosen. One disadvantage of this method is that the total wavelength span available for the WDM channels is limited by the polarisation dispersion, which is in the order of 4-5 nm for conventional InGaAsP/InP DH structures. Another disadvantage is that the exact value of the polarisation dispersion is very sensitive to variations in layer composition and thickness, which makes it difficult to obtain a good match.

Half-wave plate

A very elegant method is the insertion of a $\lambda/2$-plate in the middle of the phased array. Light entering the array in TE-polarised state will be converted by the $\lambda/2$-plate and will travel through the second half of the array in TM-polarised state, and TM-polarised light will similarly traverse half the array in TE-state. As a consequence TE- and TM-polarised input signals will experience the same phase transfer regardless of the birefringence properties of the waveguides applied. This method was introduced by Takahashi et al. [153] and using polyimide half-wave plates, it has been successfully applied to silica-based [60,91] and $LiNbO_3$-based devices [95,96]. As the polyimide half-wave plates have a thickness of more than 10 μm, they are only applicable to waveguide structures with a small NA which can bridge this distance with small diffraction losses. With semiconductor waveguides, the method is not practical due to the large NA of these waveguides. It could be applied successfully if a compact and fabrication tolerant integrated polarisation converter could be developed.

Dispersion compensation

For semiconductor-based PHASARs, a broadband solution for the polarisation dependence problem is found in compensation of the polarisation dispersion by inserting a waveguide section with a different birefringence in the phased array. This method was suggested for

silica-based waveguides by Takahashi et al. [154] and successfully applied to InP-based devices by Zirngibl et al. [183]. A more comprehensive account of this method can be found in Chapter 4.

Polarisation splitter
Another method for obtaining polarisation independence is by applying a polarisation splitter at the input, as shown in figure 2.8. Due to the polarisation dispersion, the position of the focal spot in the image plane for TE polarisation is shifted relative to the TM-polarised one. If the distance between the TE and the TM-polarised receiver waveguide in the object plane is chosen equal to the polarisation dispersion in the image plane, the TE and TM-polarised signals will focus on the same position and the response will become polarisation independent over a broad wavelength range. This method does not apply to $N \times N$ devices.

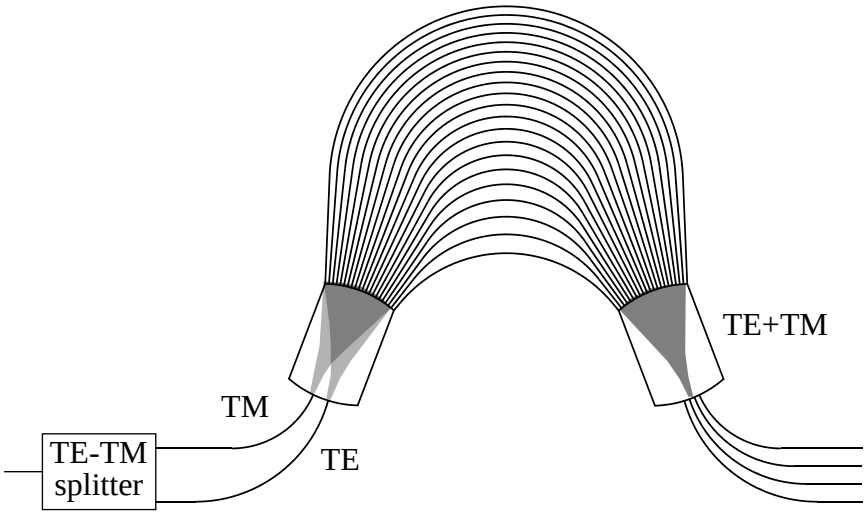

Figure 2.8 Application of a polarisation splitter at the input.

2.2.5 Design for flattened response

In many applications a flattened passband is important in order to relax the requirements on wavelength control. Three methods to achieve this goal will be discussed.

Multimode receiver waveguides
The simplest method is the use of broad (multimode) waveguides at the receiver side [6,127,129,138,139]. If the focal spot moves along these broad receiver waveguides, almost 100% of the light will be coupled into the receiver waveguide over a considerable part of the receiver waveguide aperture, thereby causing a flat region in the frequency response as shown in figure 2.9a. In this way the 1-dB bandwidth can easily be increased from 31% of the channel spacing, as shown in section 2.1.4 for a non-flattened PHASAR, to over 65%.
Due to the multimode character of the receiver waveguides, this method can only be applied at the receiver side of a WDM-link, where the multimode waveguides can be coupled to a detector without additional signal loss.

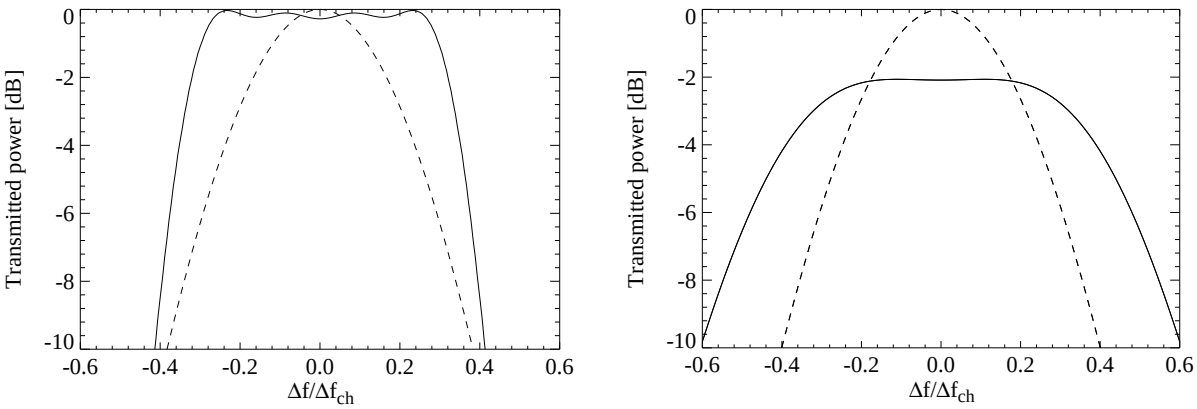

Figure 2.9 Flattening of the wavelength response by using multimode receiver waveguides (a), and by applying an MMI-powersplitter at the transmitter side (b). The dashed lines indicate the response without flattening.

MMI-flattening

A flattened response with single-mode outputs can be obtained by applying a short Multimode Interference (MMI) power splitter at the end of the transmitter waveguide [10,124,125]. This device converts the single waveguide mode at the input end of the coupler into a double image. The resulting output field pattern has a “camel-like” shape and the depth of the central depression can be controlled with the MMI width. If the image of this “camel-shaped” field moves along the single mode receiver waveguides, the response will have a flat region as shown in figure 2.9b. This method of flattening introduces insertion loss due to the mismatch between the “camel-shaped” focal field and the receiver waveguide mode.

A similar effect can be obtained by applying a Y-junction and bringing the two output branches close together in the transmitter aperture. This method, however, is less compact and less robust.

Shaping the phase transfer

As the field in the image plane is the Fourier transform of the field at the output aperture, a field which is more or less rectangular can be realised if the field at the output aperture has a $\sin(x)/x$ distribution (x measured along the aperture). Such a sinc distribution can be approximated in a discrete manner by multiplying the field at the array aperture with a function with alternating sign in such a way that the Gaussian-like field is converted into a $\sin(x)/x$-like field with positive and negative side lobes. The multiplication can be realised by inserting an additional half wavelength into the array waveguides terminating in the negative side lobe regions, or by increasing the optical length using thermo-optic or photo-elastic effects [87].

2.2.6 Design for low loss

For properly designed PHASARs realised with low-loss waveguides, the total loss is dominated by the loss occurring at the junctions between the array and the Free Propagation Region (FPR). Low losses can be obtained if the transition from the array to the FPR is adiabatical, i.e. if the gap between the waveguides reduces linearly to zero. Due to the finite

resolution of the lithographical process, the gap between the waveguides, however, will stop abruptly when the waveguides come too close together. At this discontinuity, the field coming out of the array will show a modulation which is dependent on the width of the gap between the array waveguides and on the confinement of the field in the guides. Figure 2.10 shows the field for a large and a smaller gap. Due to the ripple in the field pattern, a considerable fraction of the power will diffract into adjacent orders and be lost. On reciprocity grounds, an equal loss will occur at the input aperture.
To reduce this loss, the ripple of the output field should be reduced. This can be obtained by reducing the gap width (which requires better lithography) or by reducing the confinement of the waveguides. A disadvantage of the latter approach is that lowering the confinement increases the minimal bending radius and, consequently, increases the device size. Low confinement can be combined with small bending radii by applying a local contrast reduction near the array apertures using a double-etch process [33].

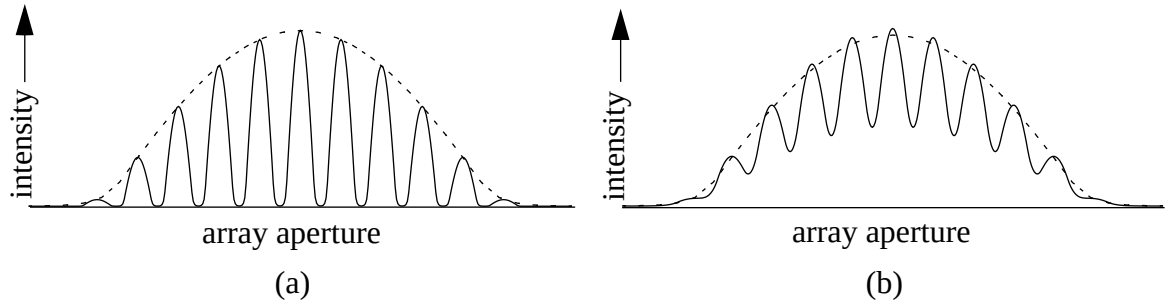

Figure 2.10 Fields at the input (dashed) and the output aperture (solid) of the phased array for a) a waveguide structure with strong confinement, and b) a structure with moderate confinement. For efficient coupling to the receiver waveguides, the output field should follow the dashed lines.

2.2.7 Device size

The relative dispersion $\tilde{D}$ of the array is defined as the displacement ds of the focal spot in the image plane with respect to the relative frequency variation δf ($\delta f = \Delta f_{ch} / f_c$), and should have the following value:

$$\tilde{D} = \frac{d_r}{\delta f} \cdot \left(1 + \frac{f}{N_{eff}} \cdot \frac{dN_{eff}}{df}\right)^{-1} \tag{2.24}$$

whereby we have assumed that $N_{eff} / N_{FPR} \approx 1$, which is valid for most waveguide structures. The relative dispersion therefore equals the derivative $dl/d\alpha$ of the array guide length with respect to the starting angle α (see equation 2.3 and 2.22, and figure 2.6), resulting in the array guide length to be written as:

$$l(\alpha) = l_o + \alpha\tilde{D} \tag{2.25}$$

The value l_o is fixed by choosing a straight section length S_r and a radius of curvature R_r at an arbitrary reference angle α_r:

$$l_o = 2S_r + \alpha_r R_r - \alpha_r \tilde{D} \tag{2.26}$$

This choice also determines the distance L between the focal points of the phased-array:

$$L = 2(S_r\cos\alpha_r + R_r\sin\alpha_r) \tag{2.27}$$

resulting in three degrees of freedom to be used for design optimisation.
Preferably, a phased-array design is made on the basis of graphs of $R(\alpha)$, $S(\alpha)$ and the guide height $H(\alpha)$ over a range of 0 to 180 degrees for different combinations of S_r and R_r. $R(\alpha)$ and $S(\alpha)$ follow directly from equations 2.19 and 2.20 by replacing α_i with α, and $H(\alpha)$ is defined as:

$$H(\alpha) = S(\alpha)\sin\alpha + R(\alpha)(1 - \cos\alpha) \tag{2.28}$$

In figure 2.11 a design example is shown using representative values. It should be noted that the phased array can only be realised if the following requirements are satisfied:

- $S(\alpha) > R_{a,min}$
- $R(\alpha) > R_{min}$
- $\frac{dH}{d\alpha}\Delta\alpha > w \cdot F$ with $2 < F < 3$

The last requirement is imposed in order to avoid the gap between the array guides becoming too small. The interval over which these requirements are satisfied must at least equal the array aperture angle θ_a. In the presented example, a value of approximately 30 degrees is found for the aperture angle θ_a ($\theta_a/\theta_o = 4$). In this case the required array aperture angle is larger than the available interval, and a phased-array demultiplexer can be realised. If this is not the case, either different combinations of S_r, R_r and α_r have to be tried, or R_a has to be reduced at the expense of a higher insertion loss for the outermost receiver waveguides ($R_a = s_{max}/\theta_{max}$ combined with equation 2.9).

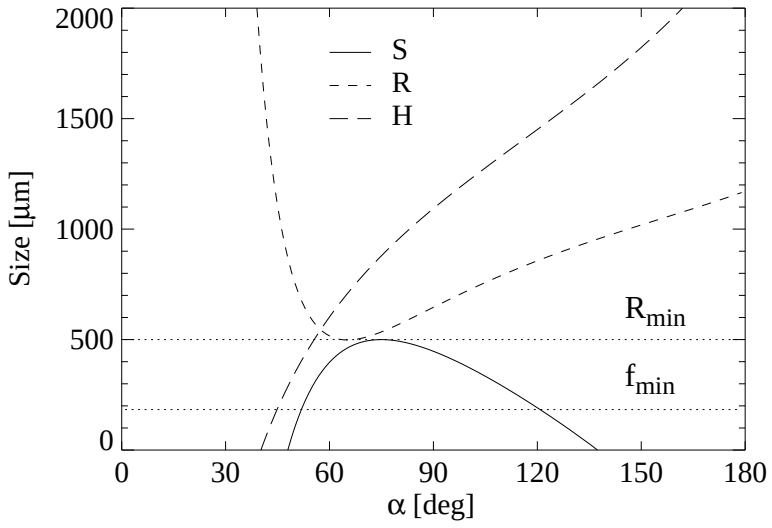

Figure 2.11 Design example for S_r = 500 μm and R_r = 500 μm at a reference radius α_r of 75 degrees.

The variation of the bending radius as a function of α can be minimised if the curve $R(\alpha)$ is flattened, which leads to a reduction of the dependence of the phased-array transfer on the radius of curvature. Flattening of the curve is done by requiring $dR/d\alpha$ and $d^2R/d\alpha^2$ to be zero at the (freely chosen) reference angle α_r. The first requirement gives a local minimum in the $R(\alpha)$ curve, whereas the latter results in a bending point in the curve, giving a larger region of α over which the curve is flat. Both requirements lead to respectively:

$$S_r = \frac{\tilde{D}}{2\tan\alpha_r} \tag{2.29}$$

and:

$$R_r = \frac{\tilde{D}}{2}\left(1 + \frac{1}{\sin^2\alpha_r}\right) \tag{2.30}$$

Unfortunately, application of this concept leads to considerable device dimensions. In the best case, $R_r = \tilde{D}$ is the smallest reference radius obtainable ($\tilde{D}$ = 2 mm is a representative value). If a concession to the flatness of the $R(\alpha)$ curve is allowed, the following empirical requirement can be used:

$$R_r = \frac{\tilde{D}}{2\sin^2\alpha_r} \tag{2.31}$$

With this condition the smallest possible reference radius is reduced by a factor two and, consequently, the device size. As small device dimensions are preferred, an adaption of the design strategy is still needed. The requirement for a flat $R(\alpha)$ curve is dropped, but in addition to the requirement of $dR/d\alpha$ to be zero at the reference angle α_r, a second requirement is imposed:

$$R_r = R_{min} \tag{2.32}$$

with R_{min} being the minimum allowed bending radius. In our case, this concept leads to the smallest device dimensions, as the minimum bending radius is in the order of only a few hundreds of microns.

The $R(\alpha)$ curve for each of the three proposed concepts is calculated using representative values for $\tilde{D}$, α_r and R_{min} of 2 mm, 75 degrees and 500 μm respectively. The graph is depicted in figure 2.12. It can be clearly seen that concept (a) ensures flatness of the $R(\alpha)$ curve over a long range of α (in this example even more than 70 degrees!), but additionally it results in the highest values for the curvature radius. Concept (b) and (c) allow for use of smaller bending radii at the cost of curve flatness. Corrections therefore have to be made in order to account for the propagation constant in the bend which depends on the curvature radius.

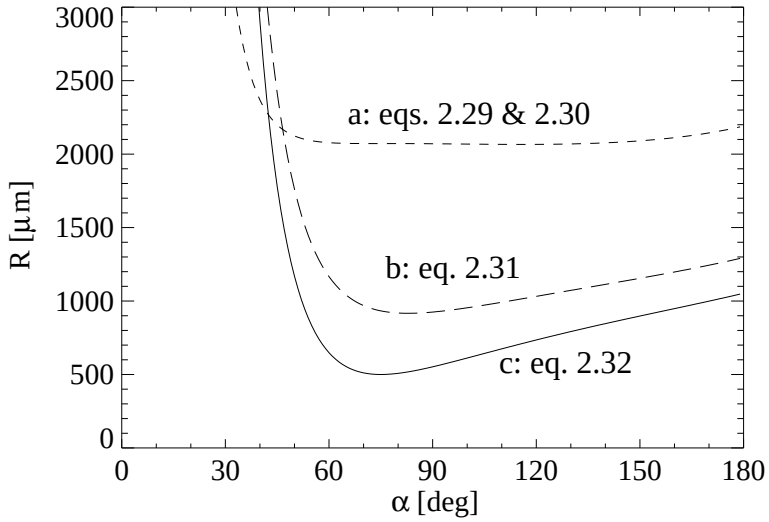

Figure 2.12 Bending radii of the array guides as a function of array guide angle α for the three proposed design concepts.

2.2.8 Correction for bending effects

In the present design concept, the curved waveguides are treated as straight waveguides with a phase transfer of $\Phi = N_{\text{eff}} k_0 2\alpha R$ and the bending radius R defined in the centre of the waveguide. With curved waveguides, however, the modal field distribution tends to shift towards the outer edge of the bend, which effectively corresponds to an increase of the bending radius. If bending radii are applied where the shift of the modal field cannot be neglected, a correction to the bending radius is needed in order to avoid degradation of the array performance. As the phase transfer of the bend with radius R seems to be caused by a bend with radius $R' = R + \Delta R$ (see figure 2.13), the corrected bending radius R' is calculated as:

$$2\alpha\beta_\phi(R) = \Phi = 2\alpha R'\beta_s \tag{2.33}$$

leading to:

$$\Delta R = \frac{\beta_\phi(R)}{\beta_s} - R \tag{2.34}$$

with β_s being the propagation constant of a straight waveguide. The apparent *increase* of the bending radius can therefore be compensated for by a *reduction* of the bending radius by the same amount, resulting in $R'' = R - \Delta R$ for the actual bending radius.
As low-loss operation is favourable, the junction losses between the straight and curved waveguides should be minimised by applying a lateral offset. The correction of the bending radius corresponds to a lateral offset in the correct direction, but in most cases it amounts to only half of the offset needed for minimum coupling loss. As the correction is in the order of a tenth of micron, the loss penalty will be negligible. It may result, however, in unwanted excitation of higher order modes, which causes “ghost” images (see section 2.1.5 and 4.4). The optimisation of the offset, both for optimum phase transfer and minimum coupling loss (or higher order mode excitation), will be explained in the next paragraph.

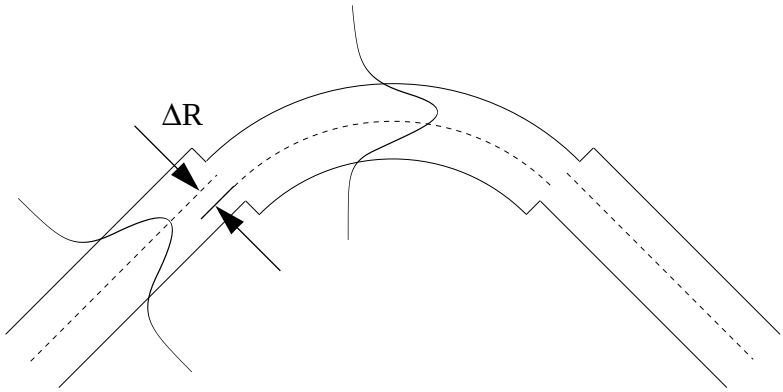

Figure 2.13 Schematic diagram of the bending correction.

2.2.9 Waveguide junctions

The correction for bending effects results in an offset at the junction of the straight and curved array waveguides, which leads to undesired effects such as coupling loss, and, in case of bimodal waveguides, also mode conversion causing “ghost” images (see section 2.1.5 and 4.4). Usually, the bending radii are chosen in such a way that the fundamental orders for both TE and TM polarisation are guided with negligible bending loss, and higher order modes with high bending loss. However, if the higher order modes are still guided with low bending loss (which is, for instance, the case for the polarisation independent raised-strip waveguides), mode conversion is undesirable. Because of different propagation constants for the fundamental and the first order mode, the resulting image will occur at a different position along the image plane. This shift can be calculated in the same way as the TE-TM shift according to equation 2.18. Mode conversion can be kept small by optimising the offset at the junctions on minimal first-order mode excitation.
Each offset between the straight and curved waveguides can be optimised separately as desired, either to maximum coupling efficiency of the fundamental mode or to minimum mode conversion. This is done by rotating each i-th straight waveguide over a small angle $\delta\alpha_i$, additional to its original angle α_i (see equation 2.21), according to:

$$\delta\alpha_i = \operatorname{asin}(\Delta x / S_i) \approx \Delta x / S_i \qquad (2.35)$$

whereby Δx is the desired lateral offset. It should be noted, that the lateral shift due to the bending correction ΔR is included in this offset and should be substracted first to find the additional rotation angle $\delta\alpha_i$. With the offset Δx in the order of a few tenths of a micron, and the straight section length S_i in the order of a few hundreds of microns, the additional angle $\delta\alpha_i$ will be very small. Additionally, in this way neither the corrected bending radius nor the length of the straight section are changed, and therefore the phase transfer of the array is not influenced.

2.3 Applications

In addition to the basic functions of wavelength multiplexing and demultiplexing, PHASARs are applied in wavelength routers and, in combination with other components such as

amplifiers and switches, in more complex devices for use in multi-wavelength networks. In this section a number of applications will be discussed further.

2.3.1 Wavelength routers

A wavelength router is obtained by designing the input and the output side of a PHASAR symmetrically, i.e. with N input and N output ports. For the cyclical rotation of the input frequencies along the output ports (as described in section 1.2), it is essential that the frequency response is periodical (as shown in figure 1.3b), which implies that the FSR should equal N times the channel spacing. From equation 2.6 it can be seen that this is obtained by choosing:

$$\Delta L = \frac{c}{N_g N \Delta f_{ch}} \tag{2.36}$$

whereby N_g is the group index of the waveguide mode, N is the number of frequency channels and Δf_{ch} is the channel spacing.
For this design, the procedure described in section 2.2.2 should be changed similarly to section 2.2.4 paragraph (ii). By fixing the incremental length according to equation 2.36 the divergence angle $\Delta\alpha$ is fixed through equation 2.3 and R_a through $R_a = d_a/\Delta\alpha$ (see figure 2.1b). With this choice of FSR, the non-uniformity L_u is fixed and will be in the order of 3 dB, which can be explained as follows. Channels at a frequency $\Delta f_{FSR}/2$ away from the central frequency will experience an excess loss L_u of at least 3 dB, because the focal spot corresponding to this frequency will be equally divided among two orders, which focus symmetrically around the centre of the image plane. As in a periodical design the frequency spacing between the outer channels comes close to the FSR, the outer channels will experience an excess loss L_u in the order of 3 dB.
Wavelength routers have been applied in various configurations in add-drop multiplexers and wavelength selective switches [47,48,64,65,90,130,143-147] and in multi-wavelength networks [54]. In combination with a DFB laser used as a wavelength converter, a wavelength router has also been applied as a wavelength switch [130, 135].

2.3.2 Multi-wavelength receivers

A multi-wavelength receiver is obtained by integration of a demultiplexer with a photodiode array. The first PHASAR receiver (reported in 1993 by Amersfoort et al. [4,5]), applied a twin-guide waveguide structure where the passive region was obtained by locally removing the absorbing top layer. Integrated receivers have also been used in buried waveguide structures [182] and in polarisation independent raised-strip waveguides [9,122]. A wavelength-flattened receiver module, hybridly integrated with a silicon bipolar front-end array, has been discussed by Steenbergen et al. [138,139,140]. Recently, a low-loss (3 dB on-chip loss) 8-channel WDM receiver with 10 GHz bandwidth per channel has been reported [141].

2.3.3 Multi-wavelength lasers

Today's WDM systems use wavelength-selected or tunable lasers as sources. Multiplexing of a number of wavelengths into one fibre is done by using a power combiner or a wavelength multiplexer. Integrated multi-wavelength lasers have been produced by combining a DFB-laser array (with a linear frequency spacing) with a power combiner on a single chip [12,173,174].

Using a power combiner for multiplexing the different wavelengths into a single fibre is a very tolerant method, but it introduces a loss of $10 \cdot \log N$ dB, with N being the number of wavelength channels. The combination loss can be reduced by applying a wavelength multiplexer, at the cost, however, of more stringent requirements on control of the laser wavelengths.
An elegant solution to this problem is combining a broadband optical amplifier array with a multiplexer into a Fabry-Perot cavity as depicted in figure 2.14. This principle was first demonstrated in the MAGIC-laser [169] in a hybridly integrated form. If one of the Semiconductor Optical Amplifiers (SOAs) is excited, the device will start lasing at the passband maximum of the multiplexer channel to which the SOA is connected. In principle all SOAs can be operated and (intensity) modulated simultaneously. An important advantage of this component is that the wavelength channels are automatically tuned to the passbands of the multiplexer and coupled to the single output port with low loss.

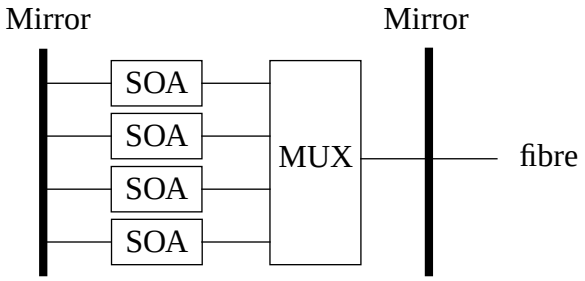

Figure 2.14 Integrated multi-wavelength laser.

Zirngibl and Joyner reported the first multi-wavelength lasers based on integration of a SOA-array with a PHASAR [68,178,179] and demonstrated it with a 9×200 Mb/s transmission experiment [180]. Despite their long cavity length, these lasers show single mode operation in a wide range of operating conditions [181]. Direct modulation speeds in excess of 1 Gb/s were reported recently [184]. Power coupled into a fibre is still low. Highest power reported so far is 0.15 mW [132,136].
Joyner et al. [70] reported integration of a MW-laser with an electro-absorption modulator. They used the power, radiated into an adjacent order of the phased array, to couple light out of the cavity into the modulator.
A problem in MW-lasers with a small FSR is that the laser may start lasing in a wrong order and, consequently, at a wrong frequency. Doerr et al. [43] proposed and demonstrated a method to suppress the transmission for undesired orders by chirping the incremental length ΔL in the array.
Tachikawa et al. [147] reported a 32-channel discretely tunable laser based on a 4×8 PHASAR with SOAs, with one reflecting mirror connected to both the 4 input and the 8 output ports. The 32 wavelengths are generated by powering the proper SOA pairs.

2.3.4 Wavelength-selective switches and add-drop multiplexers

Add-drop multiplexers (ADMs) form a special class of wavelength selective switches. They are used for coupling one or more wavelength signals from a main input port into one or more drop ports by operating the corresponding switches. The other signals are simultaneously routed into the main output port, together with the signals applied at the proper add ports. Figure 2.15a shows the configuration as produced by Tachikawa et al. [144,146,149]. The

device (hybridly integrated, whereby the switching was done by changing fibre connectors), showed a fibre-to-fibre insertion loss of 3-4 dB for the add-drop signals and 6-8 dB for the transmitted signals. Through a suitable arrangement of the loop-back optical paths, the insertion loss difference between the transmitted signals can be minimised [62].

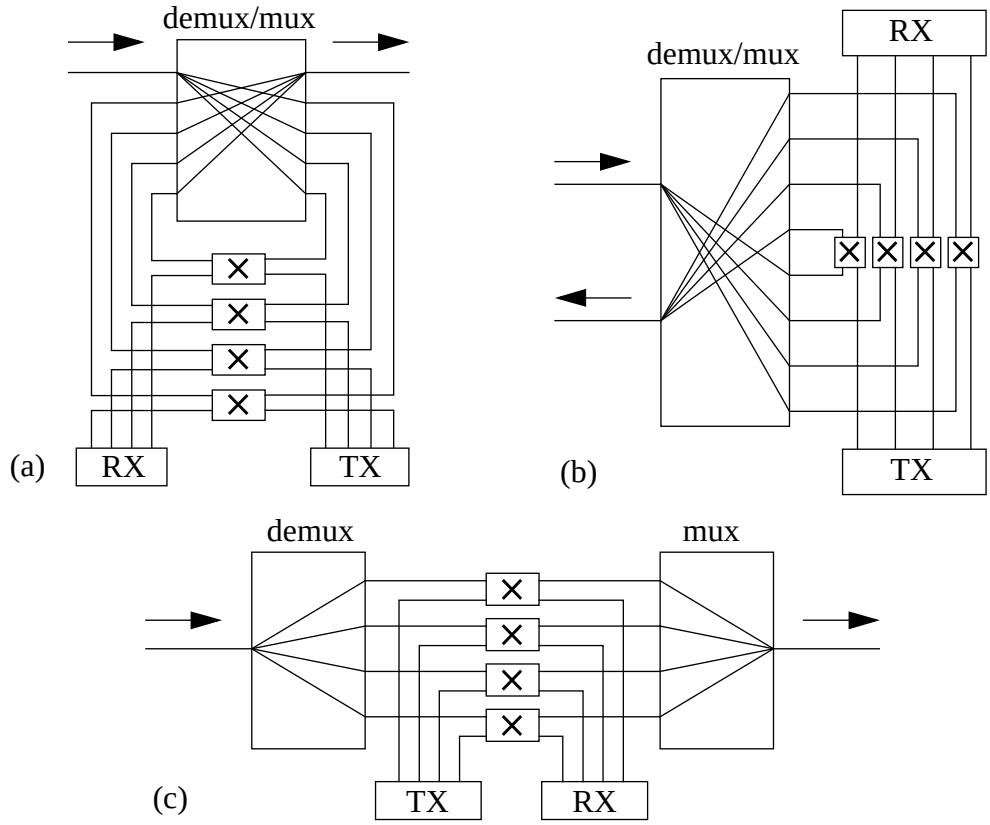

Figure 2.15 Three different ADM configurations: a) loop-back, b) fold-back, and c) cascaded demux/mux (TX = transmitter, RX = receiver, X = switch).

A disadvantage of this loop-back configuration is that the cross talk of the PHASAR is coupled directly into the main output port. This problem can be reduced by applying the PHASAR in a fold-back configuration as shown in figure 2.15b [47,64]. A third approach uses a separate demultiplexer and multiplexer (figure 2.15c) as reported by Okamoto et al. [89,90,93]. The two PHASAR used in this approach were placed close together in order to ensure that their channel frequencies match.

In wavelength routed networks, spatial switching of arbitrary wavelength signals between multiple channels allows for efficient use of the transmission capacity by using a fixed number of wavelengths and by re-using them. For this approach a number of configurations using silica-based waveguide structures have been reported [63,64,143].

The first InP-based ADM has been reported only recently [167]. The 400 GHz spaced 4-channel device (in loop-back configuration) has less than 10.7 dB on-chip loss for the pass function (including switch losses, twice the demultiplexer loss, 7 waveguide crossings, and a total of 2 cm waveguide loss). The on-chip loss for the add and drop function is less than 6.7 dB, and the cross talk is less than -20 dB for all paths. The device is extremely compact (3×6 mm^2), which demonstrates the potential for InP integration of complex circuits on a small chip area. This potential can be further developed by including optical amplifiers to compensate the on-chip losses.

A configuration which does not require switches makes use of wavelength conversion and is shown in figure 2.16 [130,135]. The modulated signal is fed into a continuously operating DBR laser, of which the wavelength can be tuned by the current injection. The insertion of the modulated signal will decrease the carrier concentration, leading to a decrease of the DBR laser signal. The output signal of the DBR laser is therefore not only converted to the DBR laser wavelength, but also inverted with respect to the input. Spatial switching can be achieved by tuning the DBR injection current and by connecting the output to a phased-array demultiplexer.

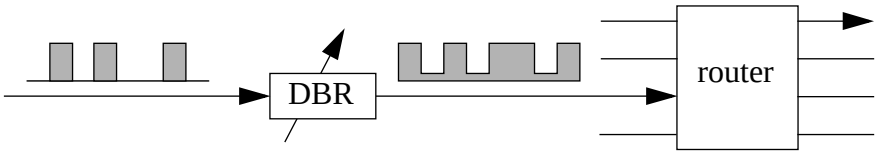

Figure 2.16 Schematic diagram of a wavelength switch employing a current-injection tunable DBR laser.

2.4 Conclusions

The range of applications of PHASAR-based devices is growing rapidly. PHASARs have proven to be flexible components which support the possibility of a broad range of functions for use in multi-wavelength networks. Silica-based devices offer the best performance and are presently being applied most widely. They might get some competition from polymer-based devices in the future. InP-based devices are most promising for manufacture of active MW-devices such as MW-lasers and receivers and, in the longer term, for more complicated circuits containing large numbers of components, such as add-drops and optical cross connects.